INJURY BIOMECHANICS RESEARCH
Proceedings of the Forty First International Workshop

Evaluation of Skull Cortical Thickness Changes with Age and Sex from Computed Tomography Scans

E.M Lillie, J.E. Urban, S.K. Lynch, A.A. Weaver, and J.D. Stitzel
Virginia Tech-Wake Forest University Center for Injury Biomechanics

ABSTRACT

Brain injuries resulting from motor vehicle crashes (MVC) are extremely common yet the details of the mechanism of injury remain to be well characterized. Skull deformation is believed to be a contributing factor to some types of traumatic brain injury (TBI). Understanding biomechanical contributors to skull deformation would provide further insight into the mechanism of head injury resulting from blunt trauma. In particular, skull thickness is thought be a very important factor governing deformation of the skull and its propensity for fracture. Previously, age and sex-based skull cortical thickness changes were difficult to evaluate based on the need for cadaveric skulls. In this study, skull thickness changes with age for each sex have been evaluated at homologous locations using a validated cortical density-based algorithm to accurately quantify cortical thickness from 123 high resolution clinical computed tomography (CT) scans. General trends indicated a slight thickening of the full skull thickness, mostly attributed to an increase in the thickness of the diploic layer. Females demonstrated a significant amount of cortical thinning for both tables of the frontal, occipital, and parietal bones ranging between a 36 and 60 percent decrease from ages 20 to 100. Males exhibited no significant changes but trends indicated a slight increase in thickness with age. Understanding how cortical and full skull thickness changes with age from a wide range of subjects can have implications in improving the biofidelity of age and sex-specific finite element models and therefore aid in the prediction and understanding of TBI from impact and blast injuries.

INTRODUCTION

It is estimated there are 1.7 million cases of traumatic brain injuries (TBI) each year, with falls and motor vehicle crashes (MVCs) being the number one and two contributors, respectively (Coronado, Xu, et al. 2011). From 2002-2006, TBI accounted for 30% of all injury-related deaths seen from emergency department visits despite the

lower injury occurrence rate of 5%. The TBIs from MVCs resulted in the largest number of TBI-related deaths (31.8%) (Faul, Xu, et al. 2010). Although studies have been conducted analyzing TBI from blunt loading conditions, more information is needed to understand the biomechanical contributors to the type and severity of TBI (Yoganandan, Gennarelli, et al. 2007, Yoganandan, Baisden, et al. 2010, Urban, Whitlow, et al. 2012). One important contributor is believed to be skull deformation. Characterizing the skull's thickness and how it changes with age is an important step toward understanding the role skull thickness plays in skull deformation.

The skull's main function is to protect the brain. It is comprised of 22 bones, 8 of which form the neurocranium and are connected by synarthrodial joints called sutures. Most of these cranial bones are categorized as flat bones and can be identified by their layered bone structure where a cancellous bone layer, called diploë, is sandwiched between two layers of dense cortical bone (cortex). These cortical layers are denoted as the inner and outer tables of the skull, as shown in Figure 1 (Saladin 2007). Previous studies have utilized cadavers and primates to evaluate the mechanical properties of the skull (McElhaney, Fogle, et al. 1970, Hubbard 1971, Hubbard, Melvin, et al. 1971, Jaslow 1990, Peterson and Dechow 2003). McElhaney et al evaluated spatial, material, and structural properties of full skull samples from cadavers (McElhaney, Fogle, et al. 1970). Skull flexural stiffness and strength was modeled by Hubbard et al using a layered beam testing technique (Hubbard 1971, Hubbard, Melvin, et al. 1971). These studies have found the flexural properties of the skull to be highly dependent on skull thickness. Cortical thickness of the outer table has been measured and reported at various locations across the skull by Peterson et al. Bone specimens were harvested from locations in the frontal, parietal, occipital, and temporal regions of the skull; the outer table was isolated and the thickness was physically measured with calipers or ultrasonic transducers. Thicknesses measured from physical specimens were found to vary within and between bones with an overall average thickness of 2.4 ± 0.8 mm (Peterson and Dechow 2002, Peterson and Dechow 2003). Additional studies have evaluated skull deformation from linear impacts concluding skull deformation can occur below mechanical failure and contribute to the occurrence and severity of TBI (Shatsky, Alter III, et al. 1974, Nusholtz, Lux, et al. 1984, Angel 2005).

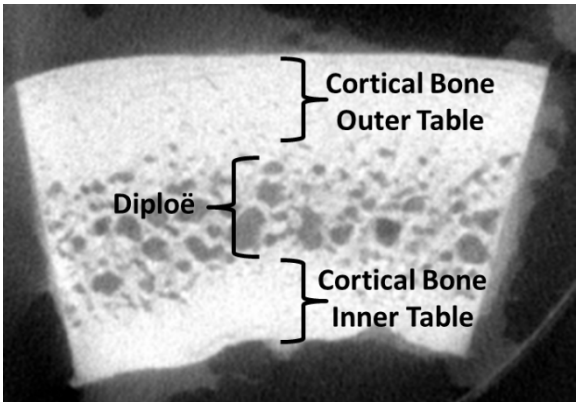

Figure 1: Cross section of microCT image of the frontal bone of a skull. Diploë is sandwiched between cortical bone tables.

The population variation seen in the reported fracture tolerance of the human skull can largely be explained by skull thickness variation and impact duration (Ruan and Prasad 2001). Ruan et al sought to quantify this variation and the effect on concussive brain injury through finite element analysis of a dynamic head impact at variable full skull thicknesses. Full skull thickness approximations for the models were based on cadaveric data in literature and developed for 5^{th}, 40^{th}, 80^{th}, and 98^{th} percentile skulls. As skull thickness increased, the peak accelerations required to reach a defined peak shear stress threshold in the brain also increased for all impact durations, where the shear stress threshold was selected as a concussive threshold based on the head injury criterion (HIC) tolerance curve (Ruan and Prasad 2001). Therefore, it is important to consider the implications of skull thickness when studying TBI.

Previous studies evaluating skull thickness have been limited by the need to physically measure samples from cadavers or primates (McElhaney, Fogle, et al. 1970, Hubbard 1971, Hubbard, Melvin, et al. 1971, Nusholtz, Lux, et al. 1984, Jaslow 1990, Peterson and Dechow 2002, Peterson and Dechow 2003, Angel 2005, Saladin 2007,

Yoganandan, Gennarelli, et al. 2007, Urban, Whitlow, et al. 2012). This study aims to improve this limitation by utilizing medical images, particularly clinical computed tomography (CT) head scans, to determine thickness measurements. The methodology presented in this study allows for the study of population-based variations in skull thickness due to age and sex. The objective of this study is to apply a cortical density method (CDM) to a large repository of clinical CT scans of subjects between ages 20 and 100 to evaluate how cortical and full skull thicknesses change with age. Trends emerging from this study could be used to better understand the relationship between cortical thickness variation and the biomechanical basis for age-related differences in head injury mechanisms.

METHODS

A total of 123 clinical head CT scans were collected from the Wake Forest Baptist Health Picture Archiving and Communication System (PACS) Radiology database. The Wake Forest University School of Medicine Institutional Review Board approved the study protocol. The in-plane resolution for each scan ranged from 0.488 to 0.625 mm with a maximum slice thickness of 0.625 mm. All scans spanned the base of the skull to the top of the skull. The ages of the subjects scanned ranged from 20 to 99 years with approximately one scan collected per year increment for both males (60 scans) and females (63 scans). Scans were visually inspected and radiology reports were reviewed to exclude skulls with anatomic or pathologic abnormalities such as skull or facial fractures, previous surgeries, congenital deformities, brain cancer, osteomyelitis, and prior TBI.

Cortical thickness of thin bone is difficult to quantify due to the resolution limitation of clinical CT scans. Thickness measurements of structures thinner than 2.5 mm are overestimated using the standard full width half max (FWHM) technique from images taken using most common clinical scan parameter (Dougherty and Newman 1999, Prevrhal, Fox, et al. 2003, Poole, Treece, et al. 2012). Recently a cortical density based method was developed to improve upon cortical thickness estimates of thin structures and this method, referred to as CDM, was recently validated by Lillie et al for skull cortical thickness estimation (Lillie, Urban, et al. 2014 (*In Review)*). To determine the cortical thickness for the subjects in this study, the CDM was applied to all 123 head CT scans. This method produced thickness measurements by optimizing the cortical density measurement from each scan when considering both in-plane and out-of-plane point spread functions (PSFs). The in-plane PSF was the spatial resolution blur and is modeled using a Gaussian curve. The out-of-plane PSF was the error associated with the orientation of the cortical bone within each imaging plane. Through the application of the CDM, a point cloud of the skull was created with over 100,000 points and associated cortical thickness values (Figure 2). The point cloud spanned the outer surface of both the inner and outer cortical tables thereby establishing cortical thickness measurements for both tables.

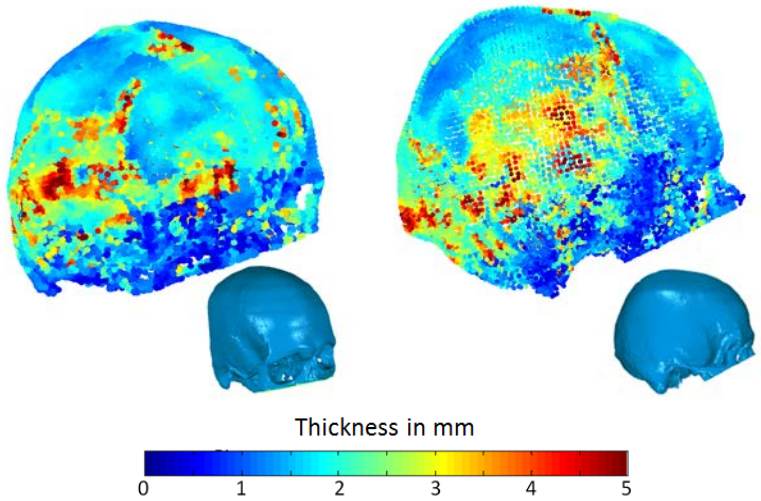

Figure 2: Point cloud of skull cortical thickness measurements collected with the CDM. Cortical thicknesses in mm are plotted with the color map for this 21 year old male.

Surface normal vectors were established at each point (x_0) in the point cloud (Figure 3). These vectors were used in relation to the skull's center of mass to differentiate between inner and outer table points on the large flat bones of the skull (Figure A1). If the normal was pointing away from the center of gravity (CG) of the head, the initial location was assumed to be on the outer table. On the contrary, if the surface normal was pointing toward the CG of the head, the initial location was assumed to be on the inner table. Successful application of the CDM was dependent on the porosity, density, and thickness of the diploë, or trabecular bone, between the two tables. In regions where the diploë was dense, thin, or low in porosity, this method was likely to estimate cortical thickness as the actual full thickness through the skull. Filtering algorithms were developed to identify locations where full thickness was measured versus cortical thickness to accurately identify the appropriate thickness measurement.

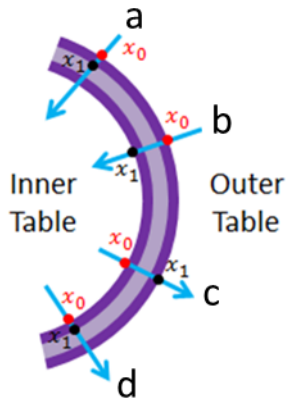

Figure 3: Schematic of thickness measurements of the skull. (a) Outer table cortical thickness measurement. (b) Full thickness measurement initialized at the outer table. (c) Full thickness measurement initialized at the inner table. (d) Inner table cortical thickness measurement.

Thickness measurements from the CDM could be one of four different types of measurements: an outer table cortical thickness measurement (Figure 3A), a full thickness measurement initiated from the outer table point cloud (Figure 3B), a full thickness measurement initiated from the inner table point cloud (Figure 3C), or an inner table cortical thickness measurement (Figure 3D). Measurements were initiated at the skull surface and were indicated by x_0 and the determined end locations were indicated as x_1. All x_0 measurements were evenly spaced on the inner and outer surface of the skull at approximately 0.8 mm resolution. The estimated thickness was the Euclidean distance between the two points. To differentiate between full thickness and cortical thickness measurements the data were filtered using an exhaustive nearest neighbor search of x_0 for all x_1 and identified the Euclidean distance between the respective x_0 and x_1 locations. Based on a study by Peterson et al., a minimum cortical thickness of 1 mm was assumed (Peterson and Dechow 2003). Given this assumption, in the case where the distance between the nearest x_0 and any end point x_1 exceeded 1 mm, the thickness measurement was assumed to be a cortical thickness measurement. In the case where x_1 was less than 1 mm from the nearest x_0 point, x_1 was considered to lie on the same skull surface as the respective x_0 value, the thickness measurement was assumed to be a full thickness measurement.

Homologous landmarks were established for each of the 123 subjects to accurately compare thickness measurements throughout the skull. The symmetric computer-aided design (CAD) data from the 50th percentile male Global Human Body Models Consortium was selected as the atlas skull geometry (Gayzik, Moreno, et al. 2011). A series of rigid, affine, and nonlinear transformations were applied to medical images developed from the CAD of the atlas skull to warp the atlas skull to each of the subject skulls (Avants and Gee 2004, Avants, Epstein, et al. 2008, Weaver, Nguyen, et al. 2013 (*In Review*)). This resulted in a series of image warps that describe the transformation between atlas space and subject space. The transformations were applied to a point cloud of 28,641 uniformly spaced landmarks (2 mm resolution) in atlas space to warp them to each subject (Weaver, Nguyen, et al. 2013 (*In Review*), Urban, Weaver, et al. 2014 (*In Review*)). Best fit alignment transformations were used to align subject thickness point clouds to each subject's homologous landmarks. The average of the nearest four subject thickness measurements to each homologous landmark was used as the smoothed thickness at that respective location. Sub-sampled point clouds of the landmarks were created for each of the main bones of the cranium from

the full skull point cloud. The reduced point clouds were created to evaluate cortical and full thickness changes of the frontal, parietal, occipital, and temporal bones. The reduced point clouds do not include thickness measurements at the sutures (Figure 4).

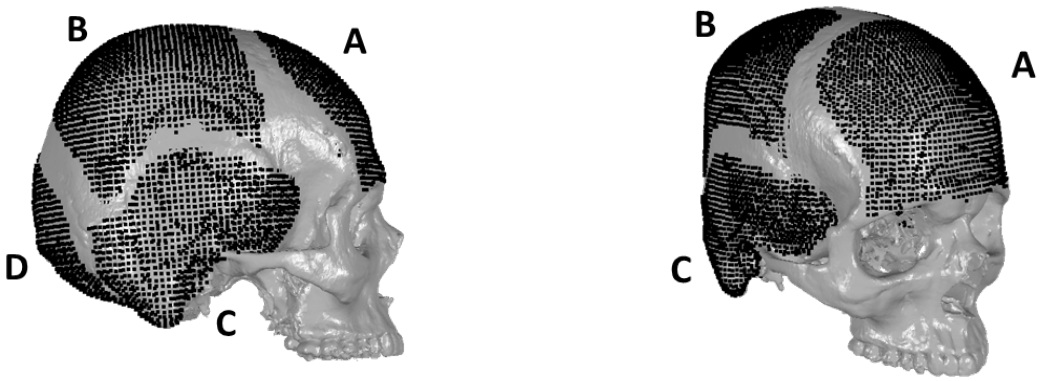

Figure 4: Sub-sampled point clouds (black) of the frontal (A), parietal (B), temporal (C), and occipital bones (D).

Additional algorithms were developed to fully distinguish full skull thickness measurements from the cortical thickness measurements. An optimization of two distance minimization algorithms was utilized to pair points on the skull surface (x_0) and calculate a full thickness measurement normal to the outer skull surface at the respective point. The first method was the application of a nearest neighbor search. Using the Euclidean distance all x_0 points on the outer table of the skull were matched to the nearest x_0 point on the inner table of the skull (Figure 5A). Full thickness measurements were calculated as the minimum distance between the two points. The second method was to determine the inner table point x_0 nearest a projected line. The surface normal unit vector for each x_0 in the outer table was used to project a line through the skull, identified as $\hat{n}$ in Figure 5B. The Euclidean distance was determined from each projected line for all of the x_0 points of the inner table. The point nearest the line projection was identified as the most likely paired point to measure full thickness perpendicular to the outer table. The optimization of these two methods enabled accurate skull surface landmark pairing to calculate the full thickness of the skull. Diploë thickness was computed as the difference between paired full thickness measurements and cortical thickness measurements in regions where it was clearly defined.

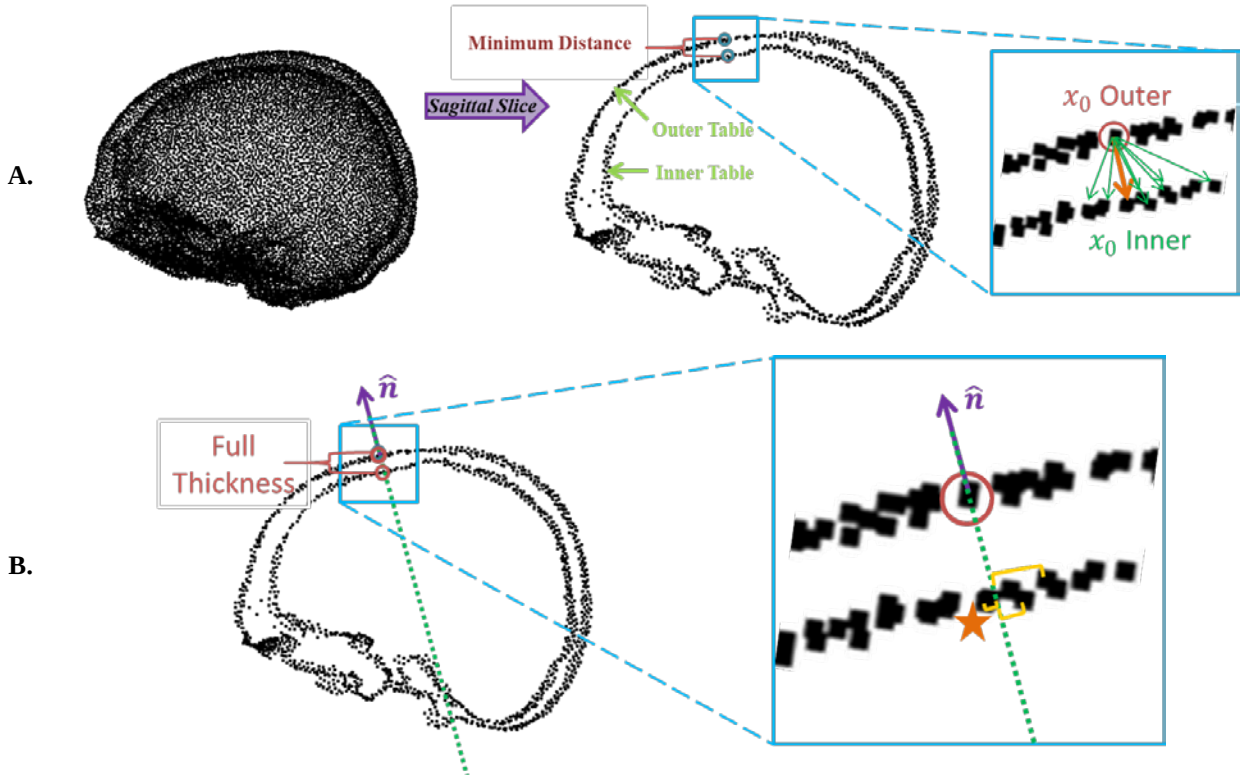

Figure 5: (A) Example from a sagittal slice of the skull point cloud demonstrating an exhaustive nearest neighbor search to find the minimum Euclidean distance between an $\boldsymbol{x_0}$ in the outer table against the $\boldsymbol{x_0}$ points of the inner table. The example pairing from such a search is marked by the bold orange arrow. (B) Example from a sagittal slice of the skull point cloud demonstrating the method in determining the nearest point of the inner table to the projected surface normal vector. The example paired landmark from this method is denoted by the orange star.

For statistical analyses, a logarithmic transformation was applied to the thickness data at the homologous landmarks to satisfy the assumptions of normality. Several approaches were used to identify potential skull thickness trends with age. Linear regressions of the log-transformed full and cortical thickness data were produced for all landmarks, as well as over averaged regions of 3 cm^2 grids. Sexual dimorphisms were evaluated through the comparison of nonlinear regressions for all subjects, males only, and females only. Statistical significance was determined using ANOVA at alpha level 0.05.

RESULTS

Cortical thickness was determined for all 123 subjects using the CDM algorithm. Through the application of the pipelined filtering and alignment algorithms, raw thickness data was evaluated at each landmark and assigned an inner or outer cortical thickness measurement, the associated full thickness calculation, and the determined thickness regressions. Resulting regressions were first evaluated for all subjects, independent of sex. Thickness and regression trends exhibited bilateral symmetry, so results are presented for the right hemisphere of the skull. In evaluating all subjects, trends are non-uniform across all landmarks and vary between and within the four main skull bones. The average trends for the entire skull indicated a slight increase in full skull thickness and a decrease in cortical bone thickness with age (Figure 6).

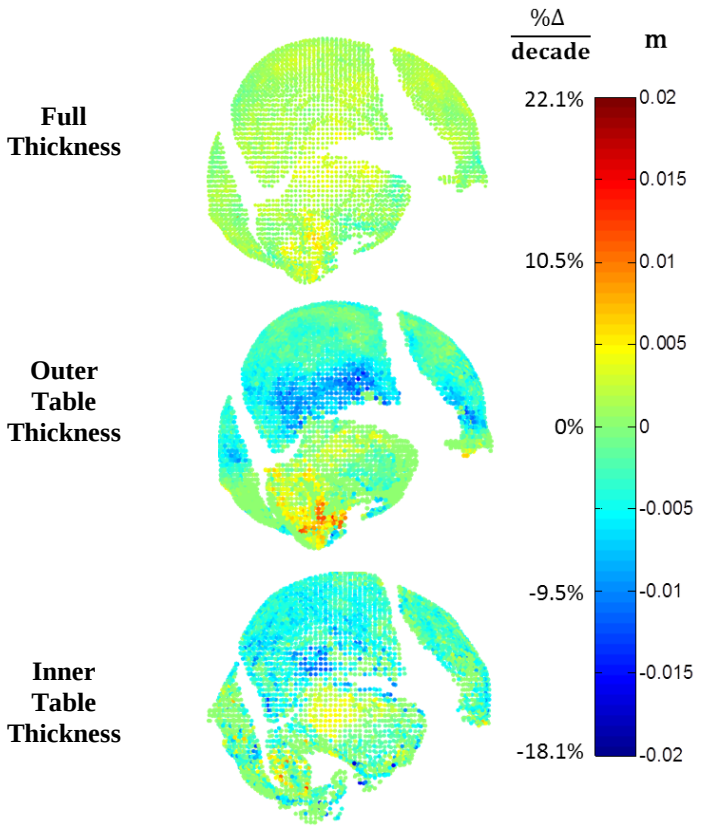

Figure 6: Color map of the nonlinear regression coefficient and associated % change (Δ) per decade of all subjects. Top to bottom: full skull thickness changes, outer table thickness changes, and inner table thickness changes.

Males and females were compared by recalculating the nonlinear regressions with sex as a differentiator. Additionally, regressions were created for all landmark data, as well as for average thickness values, spanning 3 cm^2 sections. Section-based nonlinear regression coefficients for the outer tables are shown in Figure 7. Sex-based differentiation led to the development of more distinct and significant regression trends. There was significant thinning of both the inner and outer tables for the female in the parietal, occipital and frontal bones, as indicated in Figure 7 by the blue shades representing a negative nonlinear regression coefficient. For males, cortical tables tended to increase in thickness very slightly, but not significantly. The region of the highest rate of change for the males was in the mastoid of the temporal bone. Additionally, both males and females expressed a trend toward an overall increase in skull thickness. Examples of the regressions created for the 3 cm^2 sections in Figure 7 are shown in Figure 8 at the respective region of the skull. The thinning noted in the female parietal bone with age was nearly a flat line in males indicating little to no change in thickness with age (Figure 8). The reverse was seen when considering the temporal bone, where the females expressed minimal changes while a slight increase in cortical thickness was identified in the males.

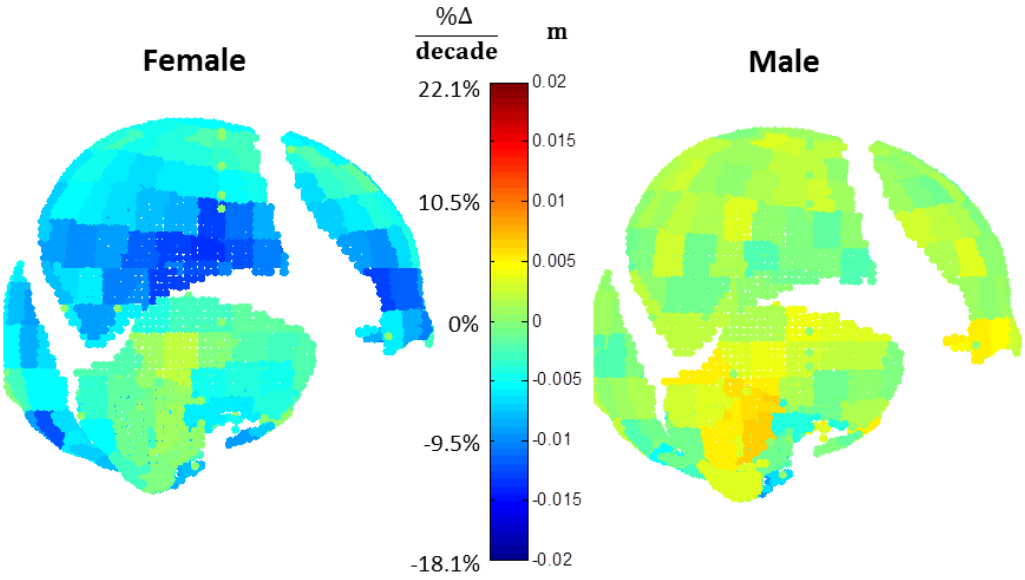

Figure 7: Female (left) and male (right) associated % change (Δ) per decade and nonlinear regression coefficients (m) for averaged 3 cm^2 sections.

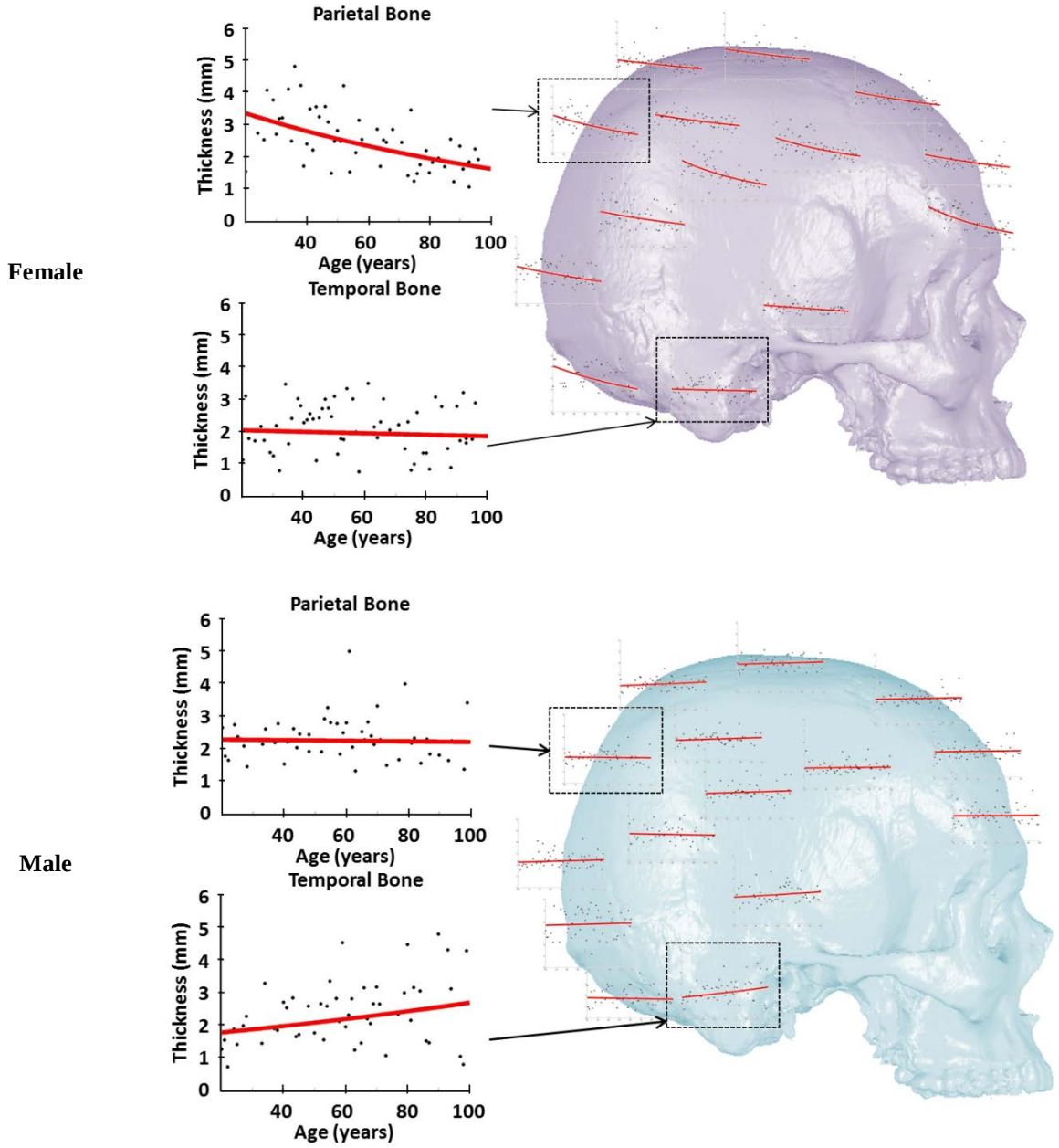

Figure 8: Representative regression trends of female (top) and male (bottom) outer table cortical thickness from 3 cm^2 sections.

CONCLUSIONS

The goal of this study was to characterize how cortical and full skull thickness measurements change with age and sex. Cortical thickness measurements were determined using the CDM algorithm and were post-processed to establish nonlinear cortical and full thickness regressions for homologous landmarks on the inner and outer tables of the skull. Significant cortical thinning was found in the outer and inner tables of the frontal, occipital, and parietal bones of females, predicting a loss between 36 and 60 percent of the original bone thickness from age 20 to

100. The males exhibited a tendency to thicken in the outer table and full thickness measurements and thin within the inner table but these changes were smaller and lacked statistical significance. These regression equations can be used in conjunction with finite element models of the head to create age- and sex-specific models for the prediction of injury.

Controlling for inter-subject variability was a major limitation in quantifying skull thickness changes with age and resulted in weak correlations for many thickness regressions. Subject scans were selected on the premise of normal bone quality from radiologic reports and visual inspection. Selection criteria did not include lifestyle information including drug use, activity level, activity type, diet, or hormone levels all of which can contribute to bone density and thickness (Chapuy, Arlot, et al. 1992, Fehling, Alekel, et al. 1995, Chakkalakal 2006, Khan and Khan 2008, Gralow, Biermann, et al. 2009). Despite the limitations, our study has provided insight into trends of skull cortical thickness changes with age and sex, providing results where previous methods in literature were too limited to characterize. These data provide a repository of high resolution thickness data for the adult skull that may be used to better understand the complex relationship between cortical thickness, skull deformation, and the resulting biomechanics of TBI-related blunt and blast impacts.

ACKNOWLEDGEMENTS

Funding was provided by the National Highway Traffic Safety Administration under Cooperative Agreement Number DTN22-09-H-00242. Views expressed are those of the authors and do not represent the views of NHTSA. The authors would like to thank Callistus Nguyen and Mimin Meliyani for assisting in data collection.

REFERENCES

ANGEL, J. L. (2005). "A new measure of growth efficiency: Skull base height." American journal of physical anthropology 58(3): 297-305.

AVANTS, B. and GEE, J. C. (2004). "Geodesic estimation for large deformation anatomical shape averaging and interpolation." Neuroimage 23 Suppl 1: S139-50.

AVANTS, B. B., EPSTEIN, C. L., GROSSMAN, M. and GEE, J. C. (2008). "Symmetric diffeomorphic image registration with cross-correlation: evaluating automated labeling of elderly and neurodegenerative brain." Med Image Anal 12(1): 26-41.

CHAKKALAKAL, D. A. (2006). "Alcohol-Induced Bone Loss and Deficient Bone Repair." Alcoholism: Clinical and Experimental Research 29(12): 2077-2090.

CHAPUY, M. C., ARLOT, M. E., DUBOEUF, F., BRUN, J., CROUZET, B., ARNAUD, S., DELMAS, P. D. and MEUNIER, P. J. (1992). "Vitamin D3 and calcium to prevent hip fractures in elderly women." New England Journal of Medicine 327(23): 1637-1642.

CORONADO, V., XU, L., BASAVARAJU, S., MCGUIRE, L., WALD, M., FAUL, M., GUZMAN, B. and HEMPHILL, J. (2011). "Surveillance for traumatic brain injury-related deaths--United States, 1997-2007." MMWR Surveill Summ 60(5): 1-32.

DOUGHERTY, G. and NEWMAN, D. (1999). "Measurement of thickness and density of thin structures by computed tomography: A simulation study." Medical Physics 26(7): 1341-1348.

FAUL, M., XU, L., WALD, M. M. and CORONADO, V. G. (2010). Traumatic brain injury in the United States: emergency department visits, hospitalizations, and deaths. Atlanta GA, Centers for Disease Control and Prevention, National Center for Injury Prevention and Control.

FEHLING, P. C., ALEKEL, L., CLASEY, J., RECTOR, A. and STILLMAN, R. J. (1995). "A comparison of bone mineral densities among female athletes in impact loading and active loading sports." Bone 17(3): 6.

GAYZIK, F. S., MORENO, D. P., GEER, C. P., WUERTZER, S. D., MARTIN, R. S. and STITZEL, J. D. (2011). "Development of a full body CAD dataset for computational modeling: a multi-modality approach." Ann Biomed Eng 39(10): 2568-83.

GRALOW, J. R., BIERMANN, J. S., FAROOKI, A., FORNIER, M. N., GAGEL, R. F., KUMAR, R. N., SHAPIRO, C. L., SHIELDS, A., SMITH, M. R. and SRINIVAS, S. (2009). "NCCN Task Force Report: Bone health in cancer care." Journal of the National Comprehensive Cancer Network 7(Suppl 3): S-1-S-32.

HUBBARD, R. P. (1971). "Flexure of layered cranial bone." Journal of Biomechanics 4(4): 251-263.

HUBBARD, R. P., MELVIN, J. W. and BARODAWALA, I. T. (1971). "Flexure of cranial sutures." Journal of Biomechanics 4(6): 491-496.

JASLOW, C. R. (1990). "Mechanical properties of cranial sutures." Journal of Biomechanics 23(4): 313-321.

KHAN, M. and KHAN, A. (2008). "Cancer treatment–related bone loss: a review and synthesis of the literature." Current Oncology 15(Supplement 1): S30.

LILLIE, E., URBAN, J., WEAVER, A., POWERS, A. and STITZEL, J. (2014). "Estimation of Skull Table Thickness with Clinical CT and Validation with MicroCT." Journal of Anatomy. *In Review*

MCELHANEY, J. H., FOGLE, J. L., MELVIN, J. W., HAYNES, R. R., ROBERTS, V. L. and ALEM, N. M. (1970). "Mechanical properties of cranial bone." Journal of Biomechanics 3(5): 495-511.

NEWMAN, D. L., DOUGHERTY, G., AL OBAID, A. and AL HAJRASY, H. (1998). "Limitations of clinical CT in assessing cortical thickness and density." Physics in Medicine and Biology 43(3): 619-626.

NUSHOLTZ, G. S., LUX, P., KAIKER, P. and JANICKI, M. A. (1984). "Head impact response : skull deformation and angular accelerations." Stapp Car Crash Conference. Twenty-Eighth. Proceedings.: 41-74.

PETERSON, J. and DECHOW, P. C. (2002). "Material properties of the inner and outer cortical tables of the human parietal bone." The Anatomical Record 268(1): 7-15.

PETERSON, J. and DECHOW, P. C. (2003). "Material properties of the human cranial vault and zygoma." Anatomical Record Part a-Discoveries in Molecular Cellular and Evolutionary Biology 274A(1): 785-797.

POOLE, K. E., TREECE, G. M., MAYHEW, P. M., VACULÍK, J., DUNGL, P., HORÁK, M., ŠTĚPÁN, J. J. and GEE, A. H. (2012). "Cortical thickness mapping to identify focal osteoporosis in patients with hip fracture." PLoS One 7(6): e38466.

PREVRHAL, S., FOX, J. C., SHEPHERD, J. A. and GENANT, H. K. (2003). "Accuracy of CT-based thickness measurement of thin structures: Modeling of limited spatial resolution in all three dimensions." Medical Physics 30(1): 1-8.

RUAN, J. and PRASAD, P. (2001). "The effects of skull thickness variations on human head dynamic impact responses." Stapp car crash journal 45: 395-414.

SALADIN, K. S. (2007). Anatomy & Physiology: The Unity of Form and Function, McGraw-Hill Companies.

SHATSKY, S. A., ALTER III, W. A., EVANS, D. E., ARMBRUSTMACHER, V. W., CLARK, G. and EARLE, K. M. (1974). "Traumatic distortions of the primate head and chest: correlation of biomechanical, radiological and pathological data." Proceedings: Stapp Car Crash Conference 18: -.

TREECE, G. M., GEE, A. H., MAYHEW, P. M. and POOLE, K. E. (2010). "High resolution cortical bone thickness measurement from clinical CT data." Med Image Anal 14(3): 276-90.

TREECE, G. M., POOLE, K. E. S. and GEE, A. H. (2012). "Imaging the femoral cortex: Thickness, density and mass from clinical CT." Medical Image Analysis 16(5): 952-965.

URBAN, J., WEAVER, A., LILLIE, E., MALDJIAN, J., WHITLOW, C. and STITZEL, J. (2014). "Evaluation of Morphological Changes in the Adult Skull with Age and Sex." Journal of Anatomy. *In Review*

URBAN, J. E., WHITLOW, C. T., EDGERTON, C. A., POWERS, A. K., MALDJIAN, J. A. and STITZEL, J. D. (2012). "Motor Vehicle Crash-Related Subdural Hematoma from Real-World Head Impact Data." Journal of Neurotrauma 29: 8.

WEAVER, A., NGUYEN, C., SCHOELL, S., MALDJIAN, J. and STITZEL, J. (2013 (*In Review*)). "Image segmentation and registration algorithm to collect thoracic skeleton landmarks for age and gender characterization." Medical Engineering and Physics.

YOGANANDAN, N., BAISDEN, J. L., MAIMAN, D. J., GENNARELLI, T. A., GUAN, Y., PINTAR, F. A., LAUD, P. and RIDELLA, S. A. (2010). "Severe-to-fatal head injuries in motor vehicle impacts." Accident Analysis & Prevention 42(4): 1370-1378.

YOGANANDAN, N., GENNARELLI, T. A., ZHANG, J., PINTAR, F. A., TAKHOUNTS, E. and RIDELLA, S. A. (2007). "Association of Contact Loading in Diffuse Axonal Injuries from Motor Vehicle Crashes." Journal of Trauma 66(2): 7.